

This is a repository copy of *Decay spectroscopy at the two-proton drip line: radioactivity of the new nuclides 160Os and 156W*.

White Rose Research Online URL for this paper:

<https://eprints.whiterose.ac.uk/205523/>

Version: Published Version

---

**Article:**

Briscoe, A.D., Page, R.D., Uusitalo, J. et al. (61 more authors) (2023) Decay spectroscopy at the two-proton drip line: radioactivity of the new nuclides 160Os and 156W. Physics Letters B. 138310. ISSN 0370-2693

<https://doi.org/10.1016/j.physletb.2023.138310>

---

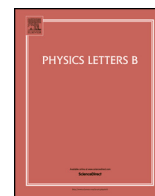
**Reuse**

This article is distributed under the terms of the Creative Commons Attribution (CC BY) licence. This licence allows you to distribute, remix, tweak, and build upon the work, even commercially, as long as you credit the authors for the original work. More information and the full terms of the licence here:

<https://creativecommons.org/licenses/>

**Takedown**

If you consider content in White Rose Research Online to be in breach of UK law, please notify us by emailing [eprints@whiterose.ac.uk](mailto:eprints@whiterose.ac.uk) including the URL of the record and the reason for the withdrawal request.



## Letter

Decay spectroscopy at the two-proton drip line: Radioactivity of the new nuclides  $^{160}\text{Os}$  and  $^{156}\text{W}$ 

A.D. Briscoe<sup>a,b,\*</sup>, R.D. Page<sup>a,b</sup>, J. Uusitalo<sup>b,a</sup>, D.T. Joss<sup>a</sup>, M.A.M. AlAqeel<sup>l,a</sup>, B. Alayed<sup>m,a</sup>, B. Andel<sup>c</sup>, S. Antalic<sup>c</sup>, K. Auranen<sup>b</sup>, H. Ayatollahzadeh<sup>d</sup>, H. Badran<sup>b</sup>, L. Barber<sup>e</sup>, G. Beeton<sup>d</sup>, M. Birova<sup>f</sup>, V. Bogdanoff<sup>b</sup>, R.M. Clark<sup>g</sup>, J.G. Cubiss<sup>h</sup>, D.M. Cullen<sup>e</sup>, J. Deary<sup>d</sup>, U. Forsberg<sup>b</sup>, T. Grahn<sup>b</sup>, P.T. Greenlees<sup>b</sup>, J.B. Hilton<sup>a,b</sup>, A. Illana<sup>b,n</sup>, H. Joukainen<sup>b</sup>, D.S. Judson<sup>a</sup>, R. Julin<sup>b</sup>, H. Jutila<sup>b</sup>, J.M. Keatings<sup>d</sup>, M. Labiche<sup>i</sup>, M. Leino<sup>b</sup>, M.C. Lewis<sup>a</sup>, J. Louko<sup>b</sup>, M. Luoma<sup>b</sup>, I. Martel<sup>a,o</sup>, A. McCarter<sup>a</sup>, P.P. McKee<sup>d</sup>, P. Mosat<sup>c</sup>, S.N. Nathaniel<sup>a</sup>, O. Neuvonen<sup>b</sup>, D. O'Donnell<sup>d</sup>, J. Ojala<sup>b</sup>, C.A.A. Page<sup>h</sup>, A.M. Plaza<sup>a,b</sup>, J. Pakarinen<sup>b</sup>, P. Papadakis<sup>i</sup>, E. Parr<sup>a</sup>, J. Partanen<sup>b,l</sup>, P. Rahkila<sup>b</sup>, P. Ruotsalainen<sup>b</sup>, M. Sandzelius<sup>b</sup>, J. Sarén<sup>b</sup>, B. Saygi<sup>j,p</sup>, J. Smallcombe<sup>a</sup>, J.F. Smith<sup>d</sup>, J. Sorri<sup>k</sup>, C.M. Sullivan<sup>a</sup>, S. Szewc<sup>b</sup>, H. Tann<sup>a,b</sup>, A. Tolosa-Delgado<sup>b</sup>, E. Uusikylä<sup>b</sup>, M. Venhart<sup>f</sup>, L.J. Waring<sup>a</sup>, G. Zimba<sup>b</sup>

<sup>a</sup> Department of Physics, Oliver Lodge Laboratory, University of Liverpool, Liverpool, L69 7ZE, United Kingdom

<sup>b</sup> Accelerator Laboratory, Department of Physics, University of Jyväskylä, FI-40014 Jyväskylä, Finland

<sup>c</sup> Department of Nuclear Physics and Biophysics, Comenius University in Bratislava, 84248 Bratislava, Slovakia

<sup>d</sup> School of Computing, Engineering, and Physics Sciences, University of the West of Scotland, Paisley, PA1 2BE, United Kingdom

<sup>e</sup> Department of Physics and Astronomy, Schuster Building, The University of Manchester, Manchester, M13 9PL, United Kingdom

<sup>f</sup> Institute of Physics, Slovak Academy of Sciences, 84511 Bratislava, Slovakia

<sup>g</sup> Nuclear Science Division, Lawrence Berkeley National Laboratory, Berkeley, CA 94720, United States of America

<sup>h</sup> School of Physics, Engineering and Technology, The University of York, York, YO10 5DD, United Kingdom

<sup>i</sup> Science and Technology Facilities Council, Daresbury Laboratory, Warrington WA4 4AD, United Kingdom

<sup>j</sup> Ankara University, Institute of Nuclear Sciences, Ankara, Türkiye

<sup>k</sup> Sodankylä Geophysical Observatory, University of Oulu, FIN-99600 Sodankylä, Finland

<sup>l</sup> Physics Department, Imam Mohammad Ibn Saud Islamic University (IMISU), P.O. Box 90950, Riyadh, 11623, Saudi Arabia

<sup>m</sup> Department of Physics, College of Science and Art at Rass-Qassim University, 53-51921, Saudi Arabia

<sup>n</sup> Departamento de Estructura de la Materia, Física Térmica y Electrónica and IPARCOS, Universidad Complutense de Madrid, E-28040 Madrid, Spain

<sup>o</sup> Faculty of Experimental Sciences, University of Huelva, 21071 Huelva, Spain

<sup>p</sup> Turkish Energy Nuclear and Mineral Research Agency, Nuclear Energy Research Institute, Ankara, Türkiye

## ARTICLE INFO

Editor: B. Blank

## ABSTRACT

The radioactivity of  $^{160}\text{Os}_{84}$  and  $^{156}\text{W}_{82}$  that lie at the two-proton drip line has been measured in an experiment performed at the Accelerator Laboratory of the University of Jyväskylä. The  $^{160}\text{Os}$  nuclei were produced using fusion-evaporation reactions induced by a beam of 310 MeV  $^{58}\text{Ni}$  ions bombarding a  $^{106}\text{Cd}$  target. The  $^{160}\text{Os}$  ions were separated in flight using the recoil separator MARA and implanted into a double-sided silicon strip detector, which was used to measure their decays. The  $\alpha$  decays of the ground state of  $^{160}\text{Os}$  ( $E_\alpha = 7092(15)$  keV,  $t_{1/2} = 97^{+97}_{-32}$   $\mu\text{s}$ ) and its isomeric state ( $E_\alpha = 8890(10)$  keV,  $t_{1/2} = 41^{+15}_{-9}$   $\mu\text{s}$ ) were measured, allowing the excitation energy of the isomer to be determined as 1844(18) keV. These  $\alpha$ -decay properties and the excitation energy of the isomer are compared with systematics. The  $\alpha$  decays were correlated with subsequent decays to investigate the  $\beta$  decays of the ground state of  $^{156}\text{W}$ , revealing that unlike its isotones, both low-lying isomers were populated in its daughter nuclide,  $^{156}\text{Ta}$ . An improved value for the half-life of the proton-decaying high-spin isomeric state in  $^{156}\text{Ta}_{83}$  of  $333^{+25}_{-22}$  ms was obtained in a separate experiment using the same experimental systems with a

\* Corresponding author at: Department of Physics, Oliver Lodge Laboratory, University of Liverpool, Liverpool, L69 7ZE, United Kingdom.

E-mail address: [adbriscoe@liverpool.ac.uk](mailto:adbriscoe@liverpool.ac.uk) (A.D. Briscoe).

<sup>1</sup> Deceased.

$^{102}\text{Pd}$  target. This result was employed to improve the precision of the half-life determined for  $^{156}\text{W}$ , which was measured as  $157^{+57}_{-34}$  ms.

## 1. Introduction

The search for new nuclides has been an ongoing endeavour throughout the history of nuclear physics, resulting in the discovery of around 3000 species to date and providing many insights into nuclear properties [1]. For odd- $Z$  elements, the direct emission of a single proton generally determines the limits of observable nuclei [2] but for even- $Z$  nuclei, pairing interactions reduce the  $Q$  values for proton emission. Consequently,  $\alpha$  radioactivity is the principal decay mode of the most neutron-deficient known isotopes of even- $Z$  elements from plutonium ( $Z = 94$ ) down to osmium ( $Z = 76$ ). The strong dependence of the  $\alpha$ -particle tunnelling probability on the  $Q_\alpha$  value means that half-lives drop rapidly with increasing neutron deficiency at the limits of known nuclei. Prior to the present work the most neutron-deficient known Os isotope was  $^{161}\text{Os}$ , which  $\alpha$  decays to  $^{157}\text{W}$  with a half-life of  $640(60)$   $\mu\text{s}$  [3]. The next even- $Z$  element below Os is tungsten ( $Z = 74$ ). Its lightest known isotopes are  $^{158}\text{W}_{84}$ , which is an  $\alpha$  emitter with a half-life of  $\sim 1$  ms [4–6], and  $^{157}\text{W}$ , which undergoes  $\beta$  decay with a half-life of  $275(40)$  ms [3]. For even lighter elements,  $\beta$  decay continues as the dominant decay mode of the most neutron-deficient even- $Z$  isotopes until the island of  $\alpha$ -particle emission above  $^{100}\text{Sn}$  is reached. Here,  $\alpha$  decay again dominates for the lightest known isotopes of xenon ( $Z = 54$ ) and tellurium ( $Z = 52$ ) [7–11].

The reason for this abrupt change in decay mode for the W isotopes is that the emission of an  $\alpha$  particle from  $^{157}\text{W}$  would involve the removal of a neutron from the  $N = 82$  core, which impacts on the  $Q_\alpha$  value [12]. Similar decreases in  $Q_\alpha$  values can be expected for its heavier isotones. Consequently,  $^{160}\text{Os}$  is expected to be the lightest osmium isotope for which  $\alpha$ -particle emission is the dominant ground-state decay mode [12]. Even more neutron-deficient Os isotopes are expected to undergo  $\beta$  decay, until the boundary of the nuclear landscape is ultimately reached with the advent of dominant two-proton emission from nuclear ground states [13,14].

The  $N = 84$  isotones are also of interest because several of them have  $\alpha$ -decaying spin-gap isomers [4–6]. In-beam spectroscopy experiments have shown that the yrast  $\nu f_{7/2} h_{9/2}$   $8^+$  states in  $^{156}\text{Hf}$  and  $^{158}\text{W}$  are at lower excitation energies than their respective  $6^+$  states and as a consequence they are isomeric [15,16]. This lowering in energy of the  $8^+$  states is also evident from systematics of level excitation energies along isotopic chains [17]. Similarly, the  $\pi h_{11/2}^n \otimes \nu f_{7/2} h_{9/2}$   $25/2^-$  state in  $^{155}\text{Lu}$  is also isomeric, lying below the  $23/2^-$  state [18,19]. In all 3 isotones, the occurrence of isomerism is attributed to the lowering in energy of configurations involving neutrons in the  $\nu h_{9/2}$  orbital relative to those in the  $\nu f_{7/2}$  orbital as the occupancy of the  $\pi h_{11/2}$  orbital increases with increasing  $Z$  above  $Z = 64$ .

The excitation energies of the  $8^+$  isomers in  $^{156}\text{Hf}$  and  $^{158}\text{W}$  are  $1959(1)$  keV [5] and  $1888(8)$  keV [6], respectively, and it is plausible that a similar isomer could also exist in  $^{160}\text{Os}$ . As well as decay by  $\alpha$ -particle emission, there is also the possibility of a two-proton decay branch from this isomer, since the ground state of  $^{160}\text{Os}$  is predicted to be unbound with  $Q_{2p} = 0.75$  MeV [12]. From the empirical formula of Ref. [20], this value is probably too low for  $2p$  emission to be observed from the ground state and the osmium isotopes that are candidates for dominant  $2p$  emission lie considerably further from stability [13]. The feasibility of observing  $2p$  decays from the isomer will depend on how much its excitation energy adds to the  $Q_{2p}$  value, balanced against the hindrance arising from the larger spin change involved in the decay.

Observing  $^{160}\text{Os}$   $\alpha$  decays would also provide an opportunity to investigate for the first time the decay properties of the ground state of its daughter nuclide,  $^{156}\text{W}$ . Although the ground state of  $^{156}\text{W}$  is also predicted to be unbound to  $2p$  emission,  $\beta$  decay is expected to dominate

[12]. The  $\beta$  decays of the lighter  $N = 82$  isotones  $^{148}\text{Dy}$ ,  $^{150}\text{Er}$  and  $^{152}\text{Yb}$  are dominated by allowed Gamow-Teller transitions to a single  $1^+$  state in their respective odd-odd daughter nuclei, followed by  $E1$   $\gamma$ -ray transitions to the  $2^-$  ground states [21–23]. These daughter nuclei also have a  $\beta$ -decaying high-spin  $\pi h_{11/2} \otimes \nu f_{7/2}$   $9^+$  isomer, but this has only been observed when populated directly in a reaction.

The  $1^+$  states have been interpreted as being  $\pi h_{11/2} \otimes \nu h_{9/2}$  configurations lying at excitation energies of  $\sim 0.5$  MeV above  $\pi d_{3/2} \otimes \nu f_{7/2}$  ground states. For the intermediate isotone  $^{154}\text{Hf}$ , only the half-life has been determined indirectly from the time differences between  $\alpha$  decays of  $^{158}\text{W}$  and  $^{154}\text{Yb}$  [24]. In the case of  $^{156}\text{W}$ , its daughter  $^{156}\text{Ta}$  has 2 low-lying isomers with the same configurations as its isotones that are separated by only 0.1 MeV [5] and could be populated through electromagnetic decays following  $\beta$  decays to  $1^+$  states. There are distinct differences in the decay properties of these states that can provide unique signatures of their population.

This letter presents measurements of the  $\alpha$  decays of the ground state and spin-gap isomer of  $^{160}\text{Os}$ , the  $\beta$ -decay properties of  $^{156}\text{W}$  and the result of a search for the competing  $2p$ -decay branches. Both nuclides lie at the proton-rich limit of the nuclear landscape, being one proton heavier than the proton emitters  $^{159}\text{Re}$  [25] and  $^{155}\text{Ta}$  [26], which are the lightest known isotopes of these elements.

## 2. Experimental details

The experiments were performed at the Accelerator Laboratory of the University of Jyväskylä. The  $^{160}\text{Os}$  nuclei were produced in the fusion-evaporation reaction  $^{106}\text{Cd}(^{58}\text{Ni}, 4n)^{160}\text{Os}$ . The  $^{58}\text{Ni}$  beam provided by the K130 cyclotron bombarded the self-supporting isotopically enriched  $^{106}\text{Cd}$  target foil of thickness  $1$  mg/cm $^2$ . The beam energy at the front of the target of  $310$  MeV was used for a period of  $292$  hours. The average beam intensity was  $6.4$  particle nA. The energy calibration for  $\alpha$  particles was based on the  $\alpha$  decays of  $^{150,151}\text{Dy}$ ,  $^{152}\text{Er}$ ,  $^{155}\text{Lu}$ ,  $^{156}\text{Hf}$  and  $^{158}\text{Ta}$  nuclei produced in the measurement [5,27].

In separate experiments using the same setup, the proton emitter  $^{156}\text{Ta}$  was produced using the fusion-evaporation reaction  $^{102}\text{Pd}(^{58}\text{Ni}, p3n)^{156}\text{Ta}$ . The self-supporting isotopically enriched  $^{102}\text{Pd}$  target had a thickness of  $1$  mg/cm $^2$  and was bombarded with  $294$  MeV  $^{58}\text{Ni}$  ions. The irradiation time and average beam intensity were  $162$  hours and  $4.8$  particle nA. These data were used to measure the half-life of the isomeric state in  $^{156}\text{Ta}$  with improved precision, which in turn was used to extract the half-life of  $^{156}\text{W}$ . Energy calibrations for proton emitters in all experiments were obtained from proton decays of  $^{147}\text{Tm}$  and  $^{151}\text{Lu}$  nuclei produced in reactions on targets of  $^{92}\text{Mo}$  and  $^{96}\text{Ru}$ .

Protons and  $\alpha$  particles emitted at the target position during evaporation residue formation were detected using JYTube [28], which comprised 120 plastic scintillator detectors arranged in a hexagonal-cylindrical geometry. Each detector was  $2$  mm thick and was directly coupled to a silicon photomultiplier on its back surface. The efficiency of JYTube for detecting a single proton or  $\alpha$  particle was estimated to be  $\sim 70\%$ . However, JYTube is also partly sensitive to other forms of radiation (such as  $\gamma$  rays), resulting in an extra signal occasionally being registered. Since the  $^{160}\text{Os}$  nuclei would be produced via the  $4n$  evaporation channel, JYTube was used to select only evaporation residues with no more than 1 signal detected in coincidence. The use of JYTube in this way allowed nuclei produced via neutron evaporation channels to be selected from the background of nuclei produced much more strongly through evaporation channels involving the emission of several protons and/or  $\alpha$  particles.

The  $^{160}\text{Os}$  and  $^{156}\text{Ta}$  ions recoiled out of the target, passed through a carbon foil of nominal thickness  $50\text{ }\mu\text{g}/\text{cm}^2$  mounted  $\sim 10\text{ cm}$  downstream of the target to reset the ionic charge-state distribution of the evaporation residues and were transported using the recoil mass separator MARA [29–31] to the detectors situated at its focal plane. The flight time was estimated to be  $\sim 0.4\text{ }\mu\text{s}$ . The ions passed through a multi-wire proportional counter (MWPC) and were implanted into a double-sided silicon strip detector (DSSD). The energy signal in the DSSD and the time of flight between the MWPC and the DSSD allowed evaporation residues to be distinguished from beam-like particles. The ion optics of MARA were tuned for a charge state of 27 for the reaction with the  $^{106}\text{Cd}$  target. For the  $^{102}\text{Pd}$  target, charge states of 27 and 25.5 were used. In each instance this allowed for the simultaneous transmission of a total of four different charge states to the implantation detector.

The DSSD had an active area of  $128\text{ mm} \times 48\text{ mm}$  and was  $300\text{ }\mu\text{m}$  thick. The strips on its front and back surfaces were orthogonal and the strip pitch of  $0.67\text{ mm}$  on both faces provided 13824 independent pixels. The minimum time for extracting energy information from successive signals in a given strip was  $8\text{ }\mu\text{s}$ . The DSSD energy thresholds were set at  $\sim 100\text{ keV}$  to allow the observation of  $\beta$ -decay signals. Two  $500\text{-}\mu\text{m}$  thick silicon detectors, each with an active area of  $50\text{ mm} \times 70\text{ mm}$ , were mounted directly behind the DSSD and used to identify high-energy light ions arriving at the MARA focal plane that “punched through” the DSSD. These detectors allowed the background arising from these particles in the DSSD to be suppressed.

An array of 8 detectors was mounted to surround the DSSD in the upstream direction. These detectors formed the walls of a silicon “box” while the DSSD formed the base. Six of the box detectors had active areas of  $50\text{ mm} \times 50\text{ mm}$  segmented into 4 quadrants and were  $500\text{ }\mu\text{m}$  thick. These were mounted in 2 groups of 3 around the ends of the DSSD. The other 2 box detectors were mounted centrally above and below the DSSD, between the 2 groups of square box detectors, to complete the array. These 2 detectors each measured  $25\text{ mm} \times 75\text{ mm}$  and were also  $500\text{ }\mu\text{m}$  thick and segmented into 2 elements. The box detectors were assembled on a frame to complete the 4 box walls with their upstream edges aligned. These box detectors were used to suppress the background from  $\alpha$  particles and protons emitted from within the DSSD in the upstream direction, depositing only part of their energy.

All detector signals were passed to the triggerless data acquisition system [32], where they were time stamped with a precision of  $10\text{ ns}$ . The data were analysed using the GRAIN [33] software package.

### 3. Results

Searching for the new nuclide  $^{160}\text{Os}$  presents a number of challenges. First, the most favourable compound nucleus reaction to synthesise  $^{160}\text{Os}$  involves the evaporation of 4 neutrons. The cross section expected for this is likely to be only  $\sim 1\text{ nb}$ , as was found for the synthesis of the exotic nuclides  $^{166}\text{Pt}$  and  $^{170}\text{Hg}$  by the same evaporation channel [34,35]. Second, the daughter of  $^{160}\text{Os}$   $\alpha$  decays is  $^{156}\text{W}$ , which is expected to  $\beta$  decay with a predicted half-life of  $\sim 130\text{ ms}$  [12]. In principle, both of the known states in  $^{156}\text{Ta}$  could be populated following the  $\beta$  decay of  $^{156}\text{W}$  (see Fig. 1). Since  $\beta$  decays result in the deposition in the DSSD of a relatively small energy that unlike proton or  $\alpha$  decays is generally not characteristic of a nuclide’s decay, they are usually disregarded in correlation analyses. Therefore in order to identify  $^{160}\text{Os}$   $\alpha$  decays, correlations must be sought with the  $\alpha$  decays of either the ground state or the  $8^+$  isomer of  $^{156}\text{Hf}$  (populated via  $^{156}\text{Ta}$   $\beta$  decays), or with proton decays from  $^{156}\text{Ta}$  [5,36]. Correlations with the proton decays could be subject to significant background levels because the proton-energy peaks lie in the same region of the energy spectrum as  $\alpha$  particles that escape from the DSSD without depositing their full energy. This problem is exacerbated by the relatively long time interval expected between  $^{160}\text{Os}$   $\alpha$  decays and the proton or  $\alpha$  decays with which they are to be correlated.

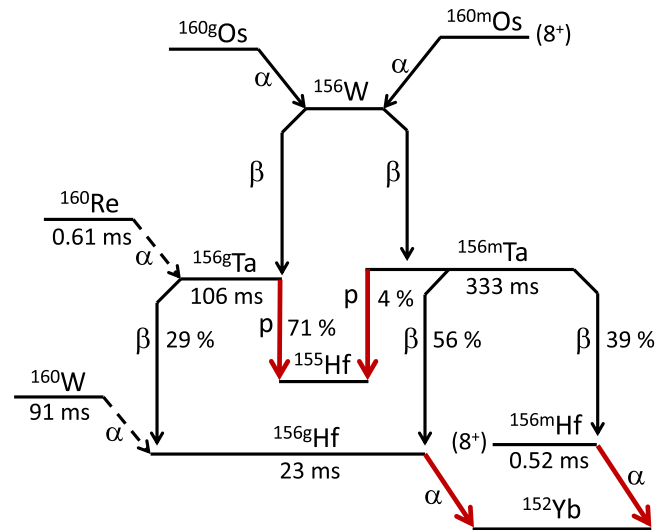
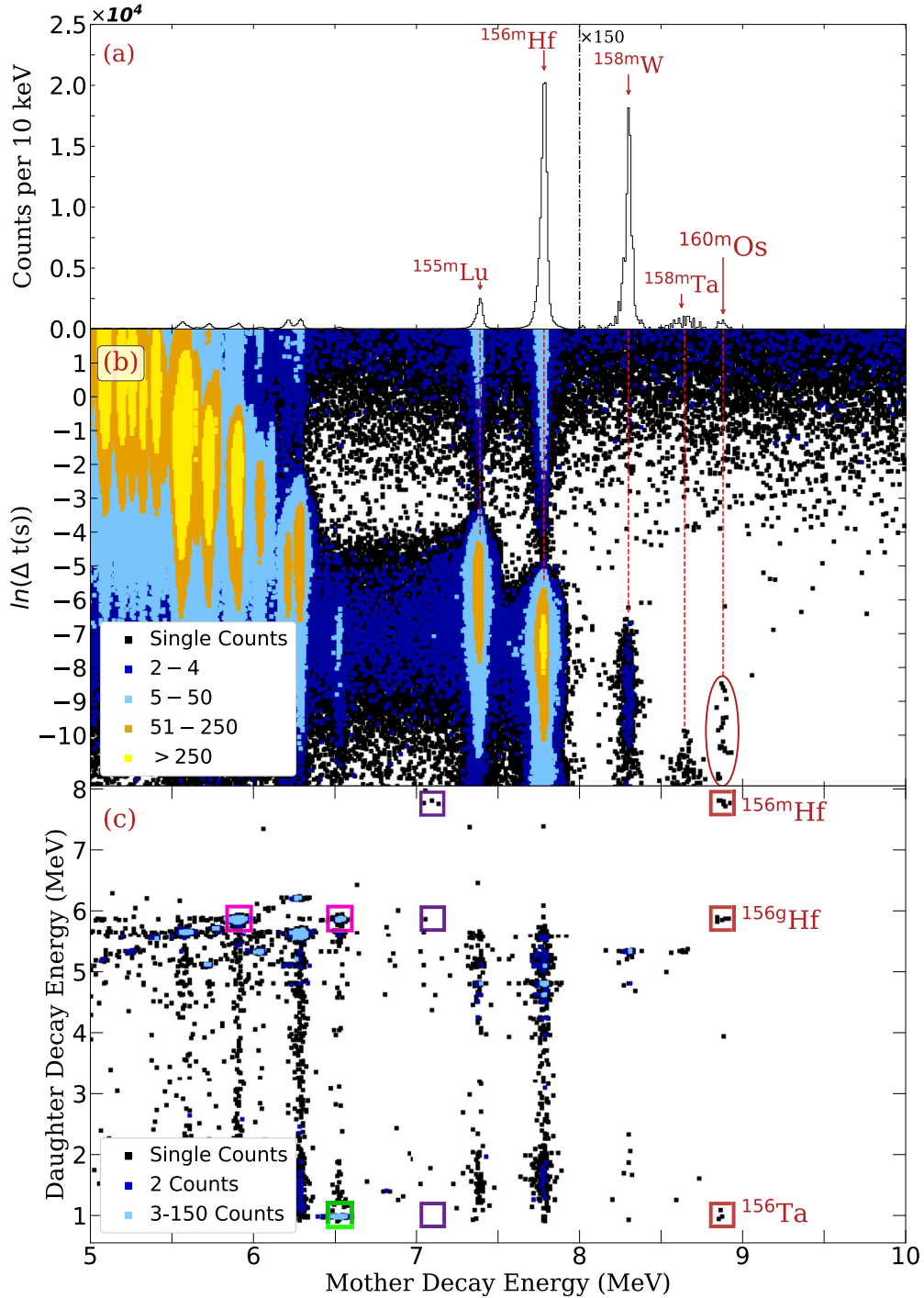


Fig. 1. Schematic diagram showing the expected  $\alpha$ -decay chain of  $^{160}\text{Os}$ . The labels  $g$  and  $m$  in the superscripts denote ground and isomeric states, respectively. The  $\alpha$  decays of both the ground state and the isomeric state of  $^{160}\text{Os}$  are expected to populate the ground state of the unknown nuclide  $^{156}\text{W}$ , which is predicted to  $\beta$  decay [12]. The red arrows denote the decays that were considered in the search for the  $\alpha$  decay of  $^{160}\text{Os}$ , namely the proton-decay branches of  $^{156}\text{Ta}$  and the  $\alpha$  decays of  $^{156}\text{Hf}$ . The dashed arrows indicate the  $\alpha$  decays of  $^{160}\text{Re}$  and  $^{160}\text{W}$ , which would be expected in correlated energy spectra together with  $^{160}\text{Os}$   $\alpha$  decays. The half-life for the isomeric state in  $^{156}\text{Ta}$  is from the present work. Other half-lives and branching ratios are taken from Refs. [5,36].

The identification of  $\alpha$  decays of the  $8^+$  isomeric state in  $^{160}\text{Os}$  should be more straightforward than those from its ground state owing to the expected high  $\alpha$ -decay energy and consequently its short half-life. Fig. 2(a) shows part of the energy spectrum of  $\alpha$  decays measured in the DSSD within  $250\text{ }\mu\text{s}$  of an evaporation residue being implanted into the same pixel, with the additional condition that no more than 1 signal was observed in JYTube. The  $^{158}\text{Ta}$  peak is noticeably broadened because its short half-life of  $6.1\text{ }\mu\text{s}$  means that its decays occur on the rapidly falling tail of the pulse of the implanted ion event [37,38]. In addition to these peaks, a new activity comprising 23 counts is visible at an energy of  $8890(10)\text{ keV}$ , which is in the energy region where  $\alpha$  decays of the  $^{160}\text{Os}$  high-spin isomer would be expected.

Fig. 2(b) shows the  $\alpha$ -decay energies plotted against the natural logarithm of the time difference between the  $\alpha$  decay and the preceding evaporation residue implanted into the same DSSD pixel. Short-lived decays appear as groups towards the bottom of this plot. These include the decays of the isomers in  $^{158}\text{Ta}$  and the  $N = 84$  isotones  $^{155}\text{Lu}$ ,  $^{156}\text{Hf}$  and  $^{158}\text{W}$ . The group of events highlighted in the ellipse are short-lived, high-energy decays that are candidates for  $\alpha$  decays of the spin-gap isomer in  $^{160}\text{Os}$ . A half-life of  $41^{+15}_{-9}\text{ }\mu\text{s}$  was extracted for this distribution, which passes the 90% confidence test outlined in ref. [39], confirming that the origin of these events is consistent with the decay of a single activity. As with other half-life values presented below, the  $8\text{ }\mu\text{s}$  dead-time period was subtracted from the individual decay times when deducing this value.

In order to assign these candidate  $\alpha$  decays to  $^{160}\text{Os}$  it is necessary to correlate them with subsequent decays as discussed above. Fig. 2(c) shows that these decays are correlated with the proton decays of  $^{156}\text{Ta}$  or the  $\alpha$  decays of either the ground state or isomeric state of  $^{156}\text{Hf}$  as expected from Fig. 1, confirming their assignment as  $\alpha$  decays of  $^{160}\text{Os}$ . Removing the constraint on the number of hits observed in JYTube does not increase the number of events in this region of the spectrum, as would be expected for a reaction channel involving only the evaporation of neutrons. The event slightly to the right of the ellipse in Fig. 2(b) is not assigned as a decay of  $^{160}\text{Os}$  because no subsequent decay event



**Fig. 2.** (a) Energy spectrum of  $\alpha$  decays measured in the DSSD within 250  $\mu\text{s}$  of an ion being implanted into the same pixel. Peaks are labelled with their assignments. Note the expanded vertical scale to the right of the dot-dash line. (b) The energies of  $\alpha$  decay plotted against the natural logarithm of the time difference between the  $\alpha$  decay and the preceding evaporation residue implanted into the same DSSD pixel. The dashed lines are drawn to guide the eye to the  $\alpha$  decays of the spin-gap isomers of  $^{155}\text{Lu}$ ,  $^{156}\text{mHf}$ ,  $^{158}\text{W}$ ,  $^{158}\text{Ta}$  and the events in the ellipse that are assigned as  $\alpha$  decays of the isomer in  $^{160}\text{Os}$ . (c) Correlation matrix of “mother”  $\alpha$ -decay events occurring within 400  $\mu\text{s}$  of an evaporation residue being implanted into the same DSSD pixel with “daughter” decays occurring within a further 1.75 s in the same pixel. Note that the minimum energy threshold was set in software to exclude  $\beta$ -decay events from these correlations. The candidate  $^{160}\text{Os}$   $\alpha$  decays can be seen to fall within the 3 groups inside the red squares corresponding to daughter proton decays of  $^{156}\text{Ta}$  and the  $\alpha$  decays of the ground state and isomeric state of  $^{156}\text{Hf}$ . The corresponding correlations of the  $\alpha$  decays of the ground state of  $^{160}\text{Os}$  are indicated by the purple squares. The green square highlights  $\alpha$  decays of  $^{160}\text{Re}$  correlated with proton decays of the ground state of  $^{156}\text{Ta}$ , while the magenta squares highlight  $\alpha$  decays of  $^{156}\text{Hf}$  that are preceded by the  $\alpha$  decays of  $^{160}\text{Re}$  and  $^{160}\text{W}$ . Note that the energy scales are valid for  $\alpha$  decays and therefore give apparent proton energies that are  $\sim 40$  keV too low.

was observed in the same DSSD pixel within 5 s of this event. Details of the measured decay energies, time differences and number of observed JYTube coincidences for the decay chains assigned to  $^{160}\text{Os}$  are presented in Table 1.

There are 3  $^{160}\text{Os}$   $\alpha$ -decay events in Fig. 2(c) correlated with  $^{156}\text{Ta}$  proton decays. Two of these have daughter decay energies that are consistent with proton emission from the ground state of  $^{156}\text{Ta}$  that is also observed following  $\alpha$  decays of  $^{160}\text{Re}$  that are highlighted by the green



**Table 1**

Data recorded for all of the decay chains assigned to  $^{160}\text{Os}$  from the present work.  $E_1$  and  $t_1$  are the energies and times after the implantation of the preceding evaporation residue into the same DSSD pixel of the  $^{160}\text{Os}$   $\alpha$  decays.  $E_n$  are the corresponding energies of the  $n^{\text{th}}$  member of the decay chain and  $t_n$  are their time after the preceding decay event in the DSSD pixel. The times  $t_n$  have not been corrected for the 8  $\mu\text{s}$  minimum observation time. However, the half-lives presented in the text have had a correction for this applied. The JYTube fold is the number of coincident signals observed in JYTube in association with the evaporation residue for each chain. Energies of decays below 2 MeV have been calibrated using the proton decays of  $^{147}\text{Tm}$  and  $^{151}\text{Lu}$ . The superscript letters denote the assignments to decays following  $^{160}\text{Os}$   $\alpha$  decays where they could be identified.

Chain #	$E_1$ (keV)	$t_1$ ( $\mu\text{s}$ )	$E_2$ (keV)	$t_2$ (ms)	$E_3$ (keV)	$t_3$ (ms)	$E_4$ (keV)	$t_4$ (ms)	$E_5$ (keV)	$t_5$ (ms)	JYTube Fold
1	8911	27	5886 <sup>a</sup>	1285	-	-	-	-	-	-	0
2	8894	31	472 <sup>h</sup>	43	165 <sup>i</sup>	1498	5883 <sup>a</sup>	55	4820 <sup>e</sup>	1139	0
3	8868	31	180 <sup>i</sup>	1605	7801 <sup>b</sup>	1	-	-	-	-	0
4	8878	205	1016 <sup>c</sup>	256	-	-	-	-	-	-	1
5	8850	15	341 <sup>h</sup>	256	5904 <sup>a</sup>	1285	-	-	-	-	0
6	8888	28	156 <sup>h</sup>	28	7741 <sup>b</sup>	923	-	-	-	-	0
7	8891	166	867 <sup>h</sup>	314	7716 <sup>b</sup>	48	-	-	-	-	0
8	8852	14	218 <sup>h</sup>	108	7811 <sup>b</sup>	662	-	-	-	-	0
9	8847	102	5839 <sup>a</sup>	864	-	-	-	-	-	-	0
10	8888	181	204 <sup>h</sup>	712	7791 <sup>b</sup>	307	1345	314	-	-	0
11	8929	27	245 <sup>h</sup>	48	7765 <sup>b</sup>	578	-	-	-	-	0
12	8851	52	425 <sup>g</sup>	312	974 <sup>c</sup>	226	215	840	-	-	0
13	8871	57	5864 <sup>a</sup>	800	-	-	-	-	-	-	0
14	8856	13	1131 <sup>d</sup>	916	5577 <sup>f</sup>	1096	-	-	-	-	1
15	7108	112	878 <sup>h</sup>	88	7812 <sup>b</sup>	70	-	-	-	-	0
16	7069	105	5879 <sup>a</sup>	489	-	-	-	-	-	-	0
17	7144	13	7756 <sup>b</sup>	82	1871	1414	4815 <sup>e</sup>	4721	-	-	0
18	7049	364	7767 <sup>b</sup>	481	-	-	-	-	-	-	1

<sup>a</sup>  $\alpha$  decay of  $^{156}\text{Hf}$  ground state.

<sup>b</sup>  $\alpha$  decay of  $^{156}\text{Hf}$  isomeric state.

<sup>c</sup> Proton decay of  $^{156}\text{Ta}$  ground state.

<sup>d</sup> Proton decay of  $^{156}\text{Ta}$  isomeric state.

<sup>e</sup>  $\alpha$  decay of  $^{152}\text{Er}$ .

<sup>f</sup>  $\alpha$  decay of  $^{155}\text{Lu}$ .

<sup>g</sup>  $\beta$  decay of  $^{156}\text{W}$  feeding  $^{156}\text{Ta}$  ground state.

<sup>h</sup>  $\beta$  decay of  $^{156}\text{W}$  feeding  $^{156}\text{Ta}$  isomeric state.

<sup>i</sup>  $\beta$  decay of  $^{156}\text{Ta}$  isomeric state.

square. The energy of the third daughter event is more than 100 keV higher, which would be consistent with proton emission from the high-spin isomeric state in  $^{156}\text{Ta}$  [5]. The next decay observed in the same DSSD pixel is consistent with it being an  $\alpha$  decay of  $^{155}\text{Lu}$ , produced via an unobserved  $\beta$  decay of  $^{155}\text{Hf}$ , confirming that this daughter event is a proton decay of  $^{156}\text{Ta}$ .

The observation of proton decays of the ground state of  $^{156}\text{Ta}$  following  $^{160}\text{Os}$   $\alpha$  decays shows that the  $\beta$  decays of  $^{156}\text{W}$  can lead to population of this state. This feeding pattern is the one observed in lighter  $N = 84$  isotones [21–23]. The decays of the ground state of  $^{156}\text{Ta}$  were studied by Darby et al., who found that the competing  $\beta$ -decay branch led to feeding of only the ground state of  $^{156}\text{Hf}$ , with a branching ratio of 29(3) % [36]. The observation of correlations of  $^{160}\text{Os}$   $\alpha$  decays with those of the isomeric state in  $^{156}\text{Hf}$  therefore confirms that the  $\beta$  decays of  $^{156}\text{W}$  also lead to population of the isomeric state in  $^{156}\text{Ta}$ , as suggested by the highest-energy  $^{156}\text{Ta}$  proton decay. The  $\beta$ -decay branches of both states in  $^{156}\text{Ta}$  populate the ground state of  $^{156}\text{Hf}$ , so the 5 observed correlations of  $^{160}\text{Os}$   $\alpha$  decays with  $\alpha$  decays of the ground state of  $^{156}\text{Hf}$  could have passed through either state in  $^{156}\text{Ta}$ . As expected from Fig. 1, correlations of  $\alpha$  decays of  $^{160}\text{W}$  and  $^{160}\text{Re}$  with those of the ground state of  $^{156}\text{Hf}$  were observed and are highlighted by the magenta squares in Fig. 2(c).

The knowledge gained from the  $\alpha$  decays of the isomeric state in  $^{160}\text{Os}$  can be used to search for the  $\alpha$  decays of its ground state. A group of 3 events, highlighted by a purple square, can be seen in Fig. 2(c) with a daughter energy consistent with  $\alpha$  decays of the  $^{156}\text{Hf}$  isomeric state. These events are assigned as  $\alpha$  decays of the ground state of  $^{160}\text{Os}$  and the half-life deduced from these 3 decays is  $107^{+147}_{-40}$   $\mu\text{s}$ . As can be seen from Table 1, the number of observed JYTube coincidences for each of

these events is compatible with an evaporation channel involving only neutrons. The other 2 purple squares indicate where the other daughter decays might be expected to appear. No events are visible where  $^{156}\text{Ta}$  proton decays would be expected, but 1 event is seen where  $^{156}\text{Hf}$  ground-state  $\alpha$  decays should occur and the evaporation residue was observed with no coincident signals in JYTube. This  $\alpha$  decay occurred 105  $\mu\text{s}$  after the implantation of an ion into the same DSSD pixel, a time difference which is consistent with the half-life deduced for the other 3  $\alpha$  decays assigned to the ground state of  $^{160}\text{Os}$ . Combining the data for all 4 decays gives a half-life of  $97^{+97}_{-32}$   $\mu\text{s}$  and an  $\alpha$ -decay energy of 7092(15) keV for the ground state of  $^{160}\text{Os}$ .

The position sensitive MWPC allowed for an analysis of the distribution of events across the MARA focal plane. It was found that the events assigned as  $\alpha$  decays of the ground state and isomeric state in  $^{160}\text{Os}$  were consistent with a nuclide with  $A = 160$ , further supporting the assignments. In addition, despite the low correlation efficiency owing to the long half-lives and high implantation rate, 2 of the chains in Table 1 also include an  $\alpha$  decay of  $^{152}\text{Er}$  that is populated following  $\beta$  decays of  $^{152}\text{Yb}$  and  $^{152}\text{Tm}$ .

It is possible to determine the half-life of  $^{156}\text{W}$  without observing its  $\beta$  decays directly, as has been done for other nuclei [24,40], provided that the decay path following the  $^{160}\text{Os}$   $\alpha$  decays is unambiguous. That means that the chains involving the  $\alpha$  decays of the  $^{156}\text{Hf}$  ground state cannot be used for this purpose because it is populated through the  $\beta$  decays of both states in  $^{156}\text{Ta}$ . Although the half-life of the ground state of  $^{156}\text{Ta}$  has been precisely measured as  $t_{1/2} = 106(4)$  ms [36], the uncertainty on the half-life of the  $^{156}\text{Ta}$  isomer is rather large ( $t_{1/2} = 375(54)$  ms) [5]. Since the majority of  $^{156}\text{W}$  decays appear to feed the isomeric state of  $^{156}\text{Ta}$ , a measurement of the half-life of this state with

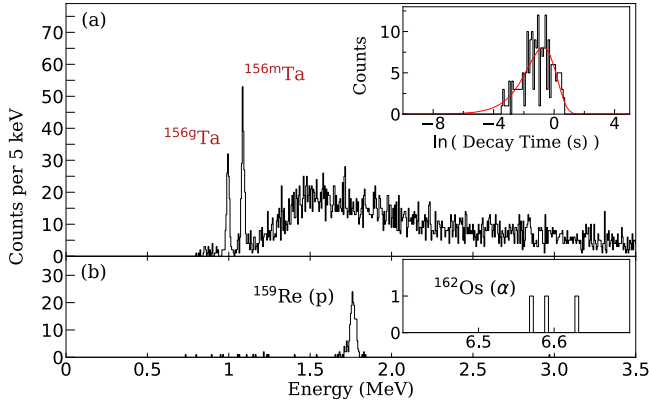


**Fig. 3.** Energy spectra of decays measured in the DSSD. Peaks are labelled with their assignments. (a) Decays that were followed by an  $\alpha$  decay of  $^{155}\text{Lu}$  in the same pixel in the measurements with the  $^{102}\text{Pd}$  target. See text for details of the timing conditions. The broad distribution extending to higher energies is from the decays of  $^{159}\text{W}$  nuclei in which the  $\alpha$  particles escape from the DSSD without depositing their full energy. The inset shows the distribution of the time differences between ions being implanted and events in the  $^{156\text{m}}\text{Ta}$  proton-decay peak in the same DSSD pixel. The red curve shows the fit to this time distribution. (b) Decays occurring within 370  $\mu\text{s}$  of an ion being implanted into the same DSSD pixel that were followed within a further 12.5 ms by an  $\alpha$  decay of  $^{158}\text{W}$  in the measurement with the  $^{106}\text{Cd}$  target. The only clear peak below 3.5 MeV is from proton decays of  $^{159}\text{Re}$ . The inset shows a higher-energy region of the spectrum, in which a few  $\alpha$  decays of  $^{162}\text{Os}$  can be seen.

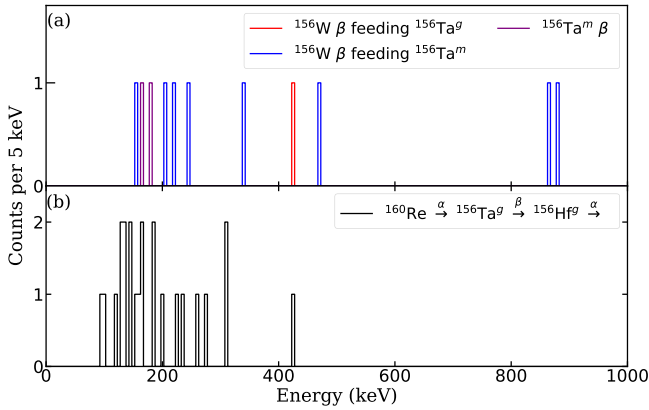


**Fig. 4.** (a) Energy spectrum of the  $\beta$ -decay events presented in Table 1. The colours indicate the assignments to specific  $\beta$ -decaying states. (b) Energy spectrum of  $\beta$  particles observed within 530 ms of an  $\alpha$  decay of  $^{160}\text{Re}$  and followed within 115 ms by an  $\alpha$  decay of the ground state of  $^{156}\text{Hf}$ .

improved precision is desirable in order to obtain a more precise half-life for  $^{156}\text{W}$ . Fig. 3(a) shows the energy spectrum from the experiment using the  $^{102}\text{Pd}$  target of events observed between 30 ms and 1875 ms of an evaporation residue being implanted into the same DSSD pixel that were then followed by a  $^{155}\text{Lu}$   $\alpha$  decay occurring between 100 ms and 5 s later. A MWPC position corresponding to a mass number of 156 was required in order to optimise the purity of the spectrum. The proton-decay peaks from the ground state and isomeric state of  $^{156}\text{Ta}$  are clearly visible. The inset shows the time differences between the ion implantation and  $^{156\text{m}}\text{Ta}$  isomer proton-decay events, plotted on a logarithmic time axis. The fitted curve is for the half-life of  $333^{+25}_{-22}$  ms deduced from these data using the method of Ref. [41].

The half-life of  $^{156}\text{W}$  was determined to be  $153^{+64}_{-39}$  ms from the time differences between  $^{160}\text{Os}$   $\alpha$  decays and subsequent  $^{156}\text{Ta}$  proton decays or  $^{156}\text{Hf}$  isomer  $\alpha$  decays, taking into account the half-lives of the intermediate  $\beta$ -decaying states. This half-life is in good agreement with the value of 130 ms predicted in Ref. [12].

It is interesting to examine the  $\beta$ -decay signals presented in Table 1 with this knowledge of the  $^{156}\text{W}$  half-life. The assignments as  $\beta$  decays of  $^{156}\text{W}$  or the ground state or isomeric state of  $^{156}\text{Ta}$  are based on the energies observed in the decay chains and/or the time differences between the signals. For example, in chains 7 and 15 the time differences between the  $\beta$  decays and the following  $\alpha$  decays of the isomer in  $^{156}\text{Hf}$  are too long to be consistent with them being decays of the  $^{156}\text{Ta}$  isomer, so they must be decays of  $^{156}\text{W}$ . The energy spectrum of the  $\beta$ -decay events presented in Table 1 is shown in Fig. 4(a), with assignments for the  $\beta$  decays they represent indicated by their colour. This can be compared with the corresponding spectrum measured for  $\beta$  decays of the ground state of  $^{156}\text{Ta}$  populated by  $\alpha$  decays of  $^{160}\text{Re}$  nuclei produced in this experiment that is shown in Fig. 4(b). The higher energies measured for chains 7 and 15 can be understood as pile-up of the energy signals of  $^{156}\text{W}$   $\beta$  particles with conversion electrons emitted in low-energy electromagnetic decays of excited states in  $^{156}\text{Ta}$ . Known transitions in  $^{156}\text{Hf}$  are not strongly converted, so  $\beta$  decays of  $^{156}\text{Ta}$  tend to produce signals of lower energy. The fraction of  $\beta$ -decay signals that were registered for  $^{156}\text{Ta}$   $\beta$  decays following  $^{160}\text{Re}$   $\alpha$  decays was 6(2) %, which is lower than appears to be the case for  $^{156}\text{W}$   $\beta$  decays. This observation is also consistent with conversion-electron emission following  $\beta$  decays of  $^{156}\text{W}$ .

The assignments of the  $\beta$ -particle signals to the decays of specific states allowed chains 2 and 5 also to be used for determining the half-life of  $^{156}\text{W}$ , thereby reducing the uncertainty compared with the value deduced above using the information only from proton- and  $\alpha$ -decay signals. Furthermore, the time differences for  $^{156}\text{W}$   $\beta$  decays themselves were used where they had been measured. Chains 1, 9, 13 and 16 that terminate with an  $\alpha$  decay of the ground state of  $^{156}\text{Hf}$  without the measurement of any  $\beta$  decays could not be used because these decay paths remained ambiguous. After applying corrections for unobserved intervening  $\beta$  decays where appropriate, a more precise value of  $157^{+57}_{-34}$  ms was determined for the half-life of  $^{156}\text{W}$ .

The data were searched for evidence of  $2p$ -decay branches from  $^{160}\text{Os}$  and  $^{156}\text{W}$ . Two-proton emission from  $^{160}\text{Os}$  would be followed by  $\alpha$  decays of  $^{158}\text{W}$  [6]. Fig. 3(b) shows the energy spectrum of decay events observed in the same DSSD pixel within 370  $\mu\text{s}$  of an evaporation residue being implanted that were followed within 12.5 ms by an  $\alpha$  decay of  $^{158}\text{W}$ . Peaks assigned as proton decays of  $^{159}\text{Re}$  [25] and  $\alpha$  decays of  $^{162}\text{Os}$  [6] are visible, but there is no other statistically significant peak that could be attributed to  $2p$  decays from  $^{160}\text{Os}$ .

If it were to occur, evidence for  $2p$  radioactivity from  $^{156}\text{W}$  would appear in Fig. 2(c), where there is a single event with a daughter energy of around 4 MeV that has a mother energy consistent with an  $\alpha$  decay of the isomeric state in  $^{160}\text{Os}$ . This energy is much higher than the predicted  $Q_{2p}$  value of 0.43 MeV for  $^{156}\text{W}$  [12], so it is more likely to be an  $\alpha$  particle emitted from  $^{156}\text{Hf}$  that escaped from the DSSD without depositing its full energy. There is also no clear sign of a peak in Fig. 2(c) in the energy region where  $^{156}\text{W}$   $2p$  decays might be expected following  $\alpha$  decays of the ground state of  $^{160}\text{Os}$ , although there are some events that are assumed to be escaping  $\alpha$  particles.

#### 4. Discussion

The  $\alpha$ -decay  $Q$  value of 7274(15) keV measured in the present work for the ground state of  $^{160}\text{Os}$  fits in well with the systematic variation of  $Q_\alpha$  values with neutron number for neutron-deficient even-even nuclides from Yb to Os. The  $Q_\alpha$  value for  $^{160}\text{Os}$  is slightly higher than would be expected from a linear extrapolation of  $Q_\alpha$  values from heavier isotopes. Such increases are also evident for the other  $N = 84$  isotones and become larger with increasing  $Z$ . Larger values are also found for  $N = 128$  isotones compared with extrapolations from their heavier isotopes [42]. In contrast, ref. [12] predicts a lower  $Q_\alpha$  value for  $^{160}\text{Os}$  than  $^{162}\text{Os}$ , although its predicted  $Q_\alpha$  values appear to be consistently overestimated for  $N = 86$  isotones.

The excitation energy of the  $\alpha$ -decaying isomer in  $^{160}\text{Os}$  determined from the difference in measured  $Q_\alpha$  values is 1844(18) keV. This value would be consistent with a continuing smooth trend in  $N = 84$  isotones of decreasing excitation energies of the yrast  $\nu f_{7/2} h_{9/2}$   $8^+$  states with increasing  $Z$  that leads to the formation of the spin-gap isomers. Extrapolating the trends of gradually increasing excitation energy with  $Z$  of the lower-spin states suggests that not only is the  $8^+$  state in  $^{160}\text{Os}$  below the  $6^+$  state but it could possibly even lie below the  $4^+$  state too.

The production cross section for the isomeric state in  $^{160}\text{Os}$  in this experiment was estimated from the yield of  $\alpha$  decays in Fig. 2(a) to be  $\sim 0.5$  nb, assuming a MARA transport efficiency of 40% and allowing for 41% of the  $\alpha$  particles escaping from the DSSD without depositing their full energy. The number of correlated decay chains for the ground state of  $^{160}\text{Os}$  was 3.5 times lower, so the combined cross section was  $\sim 0.6$  nb. This value is comparable to the value estimated for  $^{170}\text{Hg}$  [35], but is slightly lower than the cross section estimated for the production of  $^{166}\text{Pt}$  via the  $4n$  evaporation channel [34]. Substantially stronger population of the  $8^+$  isomers than the ground states in fusion-evaporation reactions was also found for the isotones  $^{156}\text{Hf}$  [15] and  $^{158}\text{W}$  [16].

Reduced  $\alpha$  widths were calculated for the decays of the two states in  $^{160}\text{Os}$  using the measured energies and half-lives [43]. A value of 60(30) keV was deduced for the ground state assuming  $\Delta\ell = 0$ , which is compatible with an unhindered  $\alpha$  decay, while assuming  $\Delta\ell = 8$  yielded a reduced alpha-decay width of 2.3(6) keV for the isomeric state. The latter value is consistent with a hindrance factor of  $\sim 20$ , as observed for the  $\alpha$  decays of the other  $N = 84$  spin-gap isomers [5].

Calculations were also performed with the Superfluid Tunnelling Model (STM) as described in Ref. [44], which has been successfully applied previously to the description of  $\alpha$  decay including that of other  $N = 84$  isotones [45,46]. The model involves the evolution of the parent nucleus, under the action of the residual nuclear interaction dominated by pairing, to a cluster-like configuration of the daughter nucleus and  $\alpha$  particle. The calculations of the ground-state  $\alpha$  decay require an estimate of the pairing gap,  $\Delta$ , and here we used the same parametrisation as discussed in Ref. [46]. The calculated value of the half-life of the ground-state decay is 55  $\mu\text{s}$ , which is to be compared to our experimental value of  $97^{+97}_{-32}$   $\mu\text{s}$ . For the isomeric state the pair gap must be reduced and the angular momentum change between initial and final states taken into account. These factors reflect the nature of the spin-gap isomers in this region. Reducing the pairing gap to 60% of the value for the ground state, and assuming  $\Delta\ell = 8$ , the calculated half-life is 13  $\mu\text{s}$ , which is to be compared with our experimental value of  $41^{+15}_{-9}$   $\mu\text{s}$ . The pairing gap for the isomer would need to be reduced to 55% of the ground-state value to reproduce the half-life. This is consistent with the systematics in Ref. [46] and reflects the observed hindrance factors of the spin-gap isomers in the  $N = 84$  isotones [5].

The decay chains of  $^{160}\text{Os}$  observed in the present work allow insights to be gleaned on the  $\beta$ -decay of  $^{156}\text{W}$ , see Fig. 1. Of the 18 chains presented in Table 1, 2 involved proton decays of  $\pi d_{3/2}$  ground state of  $^{156}\text{Ta}$ . Since the  $\beta$  decay of this state only leads to significant population of the ground state of  $^{156}\text{Hf}$  [36], the 9 chains that involved  $\alpha$  decays of the  $8^+$  isomer in  $^{156}\text{Hf}$  must have proceeded through the  $\pi h_{11/2}$  isomer in  $^{156}\text{Ta}$  [5]. In addition, there was 1 chain with proton decay from the isomer in  $^{156}\text{Ta}$ . The remaining 6 chains involved  $\alpha$  decays of the  $^{156}\text{Hf}$  ground state, which is fed in the  $\beta$  decays of both states in  $^{156}\text{Ta}$  [5]. The measured time intervals in the decay chains indicate that 2 of these proceed through the isomeric state in  $^{156}\text{Ta}$ , but the paths of the other 4 chains remain uncertain.

The present results for the  $\beta$  decay of  $^{156}\text{W}$  indicate strong feeding of the  $\pi h_{11/2}$  isomer in  $^{156}\text{Ta}$ . This behaviour is different to  $^{152}\text{Yb}$  and its lighter isotones, for which  $\beta$  decays lead predominantly to population of the  $\pi d_{3/2}$  ground state [21–23]. Multiplets of states formed by coupling the odd proton and neutron are likely to exist at low excitation energies in  $^{156}\text{Ta}$  and may open up favourable  $\gamma$ -decay paths from the  $1^+$  state to the  $\pi h_{11/2}$  isomer. Something akin to this has been observed in  $^{160}\text{Re}$ , where a  $\gamma$ -decay path from the  $\pi h_{11/2}$  isomer to the  $\pi d_{3/2}$  ground state

exists [47]. It would be interesting to investigate the  $\beta$  decays of the intermediate isotone  $^{154}\text{Hf}$  to see which decay pattern it follows and the insights this offers into the evolving structure of nuclei at the  $N = 82$  shell closure as  $Z$  increases. The statistics that could be obtained in such a study should be much higher than was possible for  $^{156}\text{W}$  in the present work and may allow the identification of  $\gamma$  rays emitted from states in  $^{154}\text{Lu}$  populated in  $^{154}\text{Hf}$   $\beta$  decays.

The empirical formula for  $2p$ -decay half-lives proposed in ref. [20] was used in that work to estimate values for superheavy nuclei. Using it for the states of interest in the present work with the  $Q_{2p}$  values from ref. [12] yields values of  $\sim 10^{66}$  s and  $\sim 10^{46}$  s for the ground states of  $^{156}\text{W}$  and  $^{160}\text{Os}$ , respectively. The corresponding values for the isomeric state in  $^{160}\text{Os}$  decaying to the ground state and isomeric state in  $^{158}\text{W}$  are  $\sim 10^{22}$  s and  $\sim 10^{48}$  s, respectively. Although one should be cautious regarding the accuracy of the predicted values, in all cases they are many orders of magnitude longer than the measured half-lives. This is consistent with the expectation that  $2p$  radioactivity from ground states will only compete with other decay modes in much lighter isotopes of these elements [13,14]. However, it is interesting to note that the predicted  $2p$ -decay half-life for the isomer in  $^{160}\text{Os}$  to the ground state of  $^{158}\text{W}$  is by far the shortest of these values, suggesting that isomers may yet provide candidates for this decay mode in heavy nuclei that could be more easily accessed experimentally.

The calculations of ref. [12] predict a drop of  $\sim 2$  MeV in the  $Q_\alpha$  value moving to  $^{159}\text{Os}$  and that  $\beta$  decay will dominate. It might be possible to measure  $\beta$ -decay properties of  $^{158,159}\text{Os}$  using a similar approach to that in the present work to measure  $^{156}\text{W}$  decays, populating the Os isotopes via the expected  $\alpha$  decays of  $^{162,163}\text{Pt}$ . This appears to be very challenging, given that the lightest currently known Pt isotope is  $^{165}\text{Pt}$  [35]. Nevertheless, a measurement of  $^{162}\text{Pt}$  would be very interesting as it is the next even-even  $N = 84$  isotone above  $^{160}\text{Os}$ . The  $Q$  value for  $2p$  emission from  $^{162}\text{Pt}$  is likely to be higher than those of  $^{156}\text{W}$  and  $^{160}\text{Os}$ , but  $2p$  emission from both its ground and isomeric states will still have to compete with  $\alpha$  decay.

## 5. Summary

The radioactive decays of  $^{160}\text{Os}$  and  $^{156}\text{W}$  have been observed for the first time. When compared with their respective lighter isotones, the  $\alpha$ -decay properties of the ground state and isomeric state in  $^{160}\text{Os}$  exhibit similar behaviour, whereas the  $\beta$  decay of  $^{156}\text{W}$  follows a different pattern of populating isomeric states in its daughter. The measurements for  $^{160}\text{Os}$  extend the knowledge of excited states in even-even isotopes across a wide range of neutron numbers, extending from  $N = 84$  to  $N = 122$  [48]. The reduced excitation energy of the isomeric  $8^+$  state in  $^{160}\text{Os}$  compared with its isotones points to the continuing importance of the interaction of  $h_{9/2}$  neutrons with  $h_{11/2}$  protons approaching the  $Z = 82$  shell closure. With the expected limit of  $\alpha$ -decaying osmium isotopes having been reached and the low production cross sections, it will be very challenging to extend decay spectroscopy measurements to even lighter osmium and tungsten isotopes.

## Declaration of competing interest

The authors declare that they have no known competing financial interests or personal relationships that could have appeared to influence the work reported in this paper.

## Data availability

The data will be made available upon reasonable request after an initial embargo period in line with the Open Data policy of the University of Jyväskylä, where the data were collected.



## Acknowledgements

Financial support for this work has been provided by the United Kingdom Science and Technology Facilities Council (STFC) through the grants ST/P004598/1, ST/V001027/1 and ST/V001035/1; the EU 7<sup>th</sup> Framework Programme “Integrating Activities - Transnational Access”, Project No.: 262010 (ENSAR); by the Slovak Research and Development Agency (Contract Nos. APVV-18-0268 and APVV-20-0532) and Slovak Grant Agency VEGA (Contract Nos. 1/0651/21 and 2/0067/21); by the Research and Development Operational Programme funded by the European Regional Development Fund, project No. ITMS code 26210120023 (20%); by the US DOE under Contract No. DE-AC02-05CH11231 (LBNL); and by the Academy of Finland under the Finnish Centre of Excellence Programme 2012-2017 (Nuclear and Accelerator Based Physics Programme at JYFL). TG acknowledges the support of the Academy of Finland, contract number 131665. JP and SS acknowledge the Academy of Finland (Finland) Grant No. 307685. M. Venhart acknowledges funding from the ESET Foundation (Slovakia). The authors would like to express their gratitude to the technical staff of the Accelerator Laboratory at the University of Jyväskylä for their support. The authors would also like to wish thanks to Paul Morrall of Daresbury Laboratory for preparation of the Cd targets and to the GSI target laboratory for providing the C-reset foils, which are highly appreciated.

## References

- [1] Michael Thoennessen, *The Discovery of the Isotopes*, Springer International Publishing, Switzerland, 2016.
- [2] B. Blank, R.D. Page, Charged-particle radioactive decays, in: I. Tanihata, et al. (Eds.), *Handbook of Nuclear Physics*, Springer Nature Singapore Pte Ltd., 2022.
- [3] L. Bianco, et al., *Phys. Lett. B* 690 (2010) 15.
- [4] S. Hofmann, et al., *Z. Phys. A* 333 (1989) 107.
- [5] R.D. Page, P.J. Woods, R.A. Cunningham, T. Davinson, N.J. Davis, A.N. James, K. Livingston, P.J. Sellin, A.C. Shotton, *Phys. Rev. C* 53 (1996) 660.
- [6] H. Mahmud, et al., *Phys. Rev. C* 62 (2000) 057303.
- [7] K. Auranen, et al., *Phys. Rev. Lett.* 121 (2018) 182501.
- [8] Y. Xiao, et al., *Phys. Rev. C* 100 (2019) 034315.
- [9] D. Seweryniak, et al., *Phys. Rev. C* 73 (2006) 061301.
- [10] S.N. Liddick, et al., *Phys. Rev. Lett.* 97 (2006) 082501.
- [11] I.G. Darby, et al., *Phys. Rev. Lett.* 105 (2010) 162502.
- [12] P. Möller, M.R. Mumpower, T. Kawano, W.D. Myers, *At. Data Nucl. Data Tables* 125 (2019) 1.
- [13] E. Olsen, M. Pfutzner, N. Birge, M. Brown, W. Nazarewicz, A. Perhac, *Phys. Rev. Lett.* 110 (2013) 222501.
- [14] M. Pfutzner, I. Mukha, S.M. Wang, *Prog. Part. Nucl. Phys.* 132 (2023) 104050.
- [15] D. Seweryniak, J. Uusitalo, P. Bhattacharyya, M.P. Carpenter, J.A. Cizewski, K.Y. Ding, C.N. Davids, N. Fotiades, R.V.F. Janssens, T. Lauritsen, et al., *Phys. Rev. C* 71 (2005) 054319.
- [16] D.T. Joss, et al., *Phys. Lett. B* 772 (2017) 703.
- [17] D.T. Joss, et al., *Phys. Rev. C* 70 (2004) 017302.
- [18] K.Y. Ding, J.A. Cizewski, D. Seweryniak, H. Amro, M.P. Carpenter, C.N. Davids, N. Fotiades, R.V.F. Janssens, T. Lauritsen, C.J. Lister, et al., *Phys. Rev. C* 64 (2001) 034315.
- [19] R.J. Carroll, et al., *Phys. Rev. C* 94 (2016) 064311.
- [20] I. Sreeja, M. Balasubramaniam, *Eur. Phys. J. A* 55 (2019) 33.
- [21] K.S. Toth, Y.A. Ellis-Akova, D.M. Moltz, R.L. Mlekodaj, *Phys. Lett. B* 117 (1982) 11.
- [22] P. Kleinheinz, K. Zuber, C. Conci, C. Protop, J. Zuber, C.F. Liang, P. Paris, J. Blomqvist, *Phys. Rev. Lett.* 55 (1985) 2664.
- [23] M.E. Estevez Aguado, et al., *Phys. Rev. C* 84 (2011) 034304.
- [24] S. Hofmann, G. Münzenberg, F. Heßberger, W. Reisdorf, P. Armbruster, *Z. Phys. A* 299 (1981) 281.
- [25] D.T. Joss, et al., *Phys. Lett. B* 641 (2006) 34.
- [26] R.D. Page, et al., *Phys. Rev. C* 75 (2007) 061302.
- [27] A. Rytz, *At. Data Nucl. Data Tables* 47 (1991) 205.
- [28] J. Henderson, et al., *J. Instrum.* 8 (2013) P04025.
- [29] J. Sarén, *The ion-optical design of the MARA recoil separator and absolute transmission measurements of the RITU gas-filled recoil separator*, Ph.D. thesis, University of Jyväskylä, 2011.
- [30] J. Sarén, J. Uusitalo, M. Leino, P.T. Greenlees, U. Jakobsson, P. Jones, R. Julin, S. Juutinen, S. Ketelhut, M. Nyman, P. Peura, P. Rahkila, C. Scholey, J. Sorri, *Nucl. Instrum. Methods Phys. Res. B* 266 (2008) 4196.
- [31] J. Uusitalo, J. Sarén, J. Partanen, J. Hilton, *Acta Phys. Pol. B* 50 (2019) 319.
- [32] I.H. Lazarus, et al., *IEEE Trans. Nucl. Sci.* 48 (2001) 567.
- [33] P. Rahkila, *Nucl. Instrum. Methods Phys. Res. A* 595 (2008) 637.
- [34] C.R. Bingham, et al., *Phys. Rev. C* 54 (1996) R20.
- [35] J. Hilton, et al., *Phys. Rev. C* 100 (2019) 014305.
- [36] I.G. Darby, et al., *Phys. Rev. C* 83 (2011) 064320.
- [37] R.J. Carroll, et al., *Phys. Rev. Lett.* 112 (2014) 092501.
- [38] R.J. Carroll, et al., *Phys. Rev. C* 93 (2016) 034307.
- [39] K.H. Schmidt, *Eur. Phys. J. A* 8 (2000) 141.
- [40] P.J. Sapp, et al., *Phys. Rev. C* 84 (2011) 054303.
- [41] Stuart L. Meyer, *Data Analysis for Scientists and Engineers*, John Wiley and Sons, Inc., New York, 1975.
- [42] Meng Wang, et al., *Chin. Phys. C* 45 (2021) 030003.
- [43] J.O. Rasmussen, *Phys. Rev.* 113 (1959) 1593.
- [44] D.M. Brink, R.A. Broglia, *Nuclear Superfluidity*, Cambridge University Press, Cambridge, 2005, and references therein.
- [45] J. Rissanen, et al., *Phys. Rev. C* 90 (2014) 044324.
- [46] R.M. Clark, et al., *Phys. Rev. C* 99 (2019) 024325.
- [47] I.G. Darby, et al., *Phys. Lett. B* 695 (2011) 78.
- [48] Z. Podolyák, et al., *Phys. Rev. C* 79 (2009) 031305(R).